JJMIE

Volume 18, Number 3, September. 2024
ISSN 1995-6665
Pages 521- 534
https://doi.org/10.59038/jjmie/180307
Editor-in-Chief: Prof. Ali M. Jawarneh

Jordan Journal of Mechanical and Industrial Engineering

Effect of Laser Surface Treatment On the Crack Growth of Al-6061 Alloy Under Impact Dynamic Load

Azhar Sabah Ameed[a,*], Farag Mahel Mohammed[b], Ahlam Luaibi Shuraiji[c]

Electromechanical Engineering Department ,University of Technology- Iraq.

Received 16 Mar 2024 *Accepted 3 May 2024*

Abstract

The effect of a laser beam on the development of cracks in an AL-6061 aluminum plate at various aspect ratios of 1:1, 1:1.5, and 1:2 was investigated in this study. The investigation adopted two clamping types: Clamped-Free-Clamped-Free and Simply-Free-Simply-Free, and supported the plate with a 5 mm crack length. The study aimed to investigate the duration it takes for cracks to propagate when subjected to the impact dynamic load after being exposed to 500 watts of laser power. Compared to the plate with an aspect ratio of 1:2 and the CFCF clamping type that was not subjected to the laser beam, the numerical results showed a 36% increase while increasing by 37% in the experimental results. Furthermore, compared to the plate that was not exposed to the laser beam and had the same boundary conditions, the clamping SFSF type of aluminum plate under dynamic load showed an increase in the number of beats that are required for crack growth of 29% according to experimental results and 28% according to numerical results. The results presented show that clamping conditions have a significant impact on the growth of cracks in the plate. It was found that a crack requires more beats to grow in a crack with an aspect ratio of 1:1 than in a crack with an aspect ratio of 1:1.5, which is larger than the aspect ratio of 1:2. Furthermore, the plate with the CFCF clamping type requires fewer pulses for the crack to grow than the plate with the SFSF clamping type. The heat of a laser beam altered the microstructure of an aluminum plate, generating residual stresses and increasing its surface hardness, thereby enhancing its crack resistance and failure resistance properties. The SEM images showed how the laser beam affected the microstructure of the sample's surface, enhancing its resistance to crack growth compared with the aluminum plate's surface, which was not exposed to the laser beam, and appears smoother.

Keywords: Laser beam, impact dynamic load, crack growth, microstructure, residual stresses.

1. Introduction

In modern industry, engineering components face increasingly complex service conditions. Traditional performance indicators fail to reflect their characteristics due to dynamic response and failure under loads, such as impact. There is an urgent need to study the dynamic mechanical behavior of materials. The service performance of damaged metal materials under impact loads becomes complicated, considering the inertial effect [1,2]. Therefore, studying the behavior and failure of metal under impact is a frontier of current scientific research [3]. The investigation of the dynamic fracture performance under shock waves of crack-damaged structures yielded a model for the propagation of shock stress waves. They verify the relationship between shock stress waves and analyze the evolution law of stress and strain in materials exposed to shock waves [4]. They looked at how heat affected the buckling load of the AL-6061 alloy and developed experimental equations to explain how the buckling load decreases with temperature [5]. Researchers have discovered that using Femto and picosecond (fs and ps) lasers can enhance the corrosion resistance of Al 6061 alloy surfaces. This method involves FS laser Nano-structuring and fs-pulsed laser deposition coating. These ultrafast lasers are effective in improving Al-based alloys' corrosive properties while being precise and causing minimal damage. The technology is widely used for surface engineering and creating durable coatings for diverse technological purposes. [6-8]. The effects of varying laser beam strength and speeds on the tensile stress of an acrylic specimen have been investigated. Stress and strain were reduced by 12.25% when the laser beam's power and speed increased. They also discovered that, when comparing various sample types, tensile strength increased by an average of 14.088% [9]. The effect of three paths laser routes on the mechanical characteristics of acrylic was examined. Additionally, the impact of laser power, speed, and fracture shape on the mechanical properties of acrylic was examined. The highest observed stress rise was approximately 28% [10]. Most recent research focuses on numerical techniques for simulating fracture problems, which is an expanding field of study [11-13]. The investigation describes the crack growth behavior, the stress intensity factor ΔK, and the relationship between applying

* Corresponding author e-mail: 50085@uotechnology.edu.iq.

the Paris equation for long cracks at low maximum stress and applying the more applicable Frost-Dugdale equation at high maximum stress [14]. The study discusses the use of the combined finite-discrete element method (FDEM) to investigate the impact failures of monolithic and laminated glass. The method involves discretizing glass into discrete elements and incorporating a finite element formulation to evaluate contact forces and structural deformation accurately. A cohesive Mode I fracture model of glass is introduced based on the FDEM theories. They also present a method to enhance computational efficiency by using a hybrid meshing approach for functionally graded materials. The effectiveness of the scaled boundary finite element formulation and the FDEM in modeling fracture and fragmentation responses of laminated glass under impact is highlighted. The results provide insights into the fracture mechanisms of glass and offer guidance for design and manufacturing processes. [15–17]. This study analyzed the fatigue failure of the TBM cutter seat under alternating loads and established a prediction model for its crack initiation life. The dangerous part of the cutter seat was identified, and its crack initiation life was analyzed numerically. The feasibility of the numerical analysis method and the correctness of the prediction model were verified [18]. A finite element model was created to study the impact force of a steel wheel on an elastic half-space. The study focused on factors like impact height, elastic modulus, and Poisson's ratio. Using the Palmgren empirical formula, the peak acceleration of the steel wheel was examined. Results showed a quadratic relationship between peak acceleration, impact height, and elastic modulus, while Poisson's ratio had minimal impact. The model demonstrated around 25% error but met engineering standards. This research aids in calculating the dynamic impact force of steel wheels on elastic surfaces [19]. They adopted 3D finite element modeling to analyze the effect of temperature and fiber orientation on a Graphite/Epoxy FRP composite beam. The research focuses on mid-plane transverse deflection and interlaminar shear stress to prevent delamination in the beam. The study shows that as temperature increases, natural frequencies decrease, and stress values rise [20]. The objective of the study is to use finite element analysis to assess the stability of slopes and design support structures for temporary roads, utilizing the FLAC3D software. Steel pipe piles are simulated using the equivalent stiffness method. The study reveals peak normal and shear stresses at specific depths, along with horizontal and vertical displacements of the pile. Stress concentrations are observed at the position of the temporary road, leading to noticeable displacements in different locations on the slope. However, a proper pile arrangement can ensure slope stability without overall shear failure [21]. An analytical model in 3D Finite Element Method (FEM) was developed to investigate how the angle of the cutter's helix affects the forces experienced during milling and the bending of walls in the process of thin-wall machining of aluminum 2024-T351. The findings indicated that increased helix angles were associated with decreased milling forces and minimized wall bending. Moreover, the use of tools with higher helix angles enhanced the quality of the machined surface [22].The study described in [23] simulated the burst pressure of specimens constructed of API X70 steel with constrained and unrestrained concentric dent-crack defects using the extended Finite Element Method (XFEM) criteria in Abaqus. To improve the prediction of crack propagation, a study examined the extension of fatigue life at critical locations and simulated the crack growth rate in military aircraft [24]. Crack growth in aluminum alloy 7075 was investigated in six different unequal load conditions during the experiment. The study's findings indicate that growth can be approximated up to the point at which the plate's surface is penetrated by the fracture [25]. To simulate fatigue failure, the study built a model and used numerical analysis to determine the age at which a rock-cutting disc will break [26].A steady stress drop would result in increased crack growth at a constant stress intensity factor ΔK, according to a study that examined the fatigue strength and crack growth behavior of AISI 304L stainless steel at room temperature [27]. The study used the elastic spring method (ESM) to simulate the presence of several cracks in a single tooth in a finite element analysis model of a gear crack with time-varying gear mesh stiffness reduction [28]. Numerical analysis in three dimensions was carried out on a thick cylinder that had a semi-elliptical crack in it. The research findings indicate that the stress intensity component is influenced by both the wall's thickness and the geometry of the crack [29]. The study looked at spot welding spot steel and how the welding tool affected the welded sample's fatigue life. It found that, depending on the kind of stresses, the welding tool had an impact of 10% to 30% [30]. The investigation focused on how heat treatments affected the fatigue life of cast alloy 7075 under low cycle conditions. The findings indicated that the treatment exhibited a stronger resistance to crack propagation [31]. The study examined the fatigue stress of three functionally graded materials (FGMs) using experimental testing and numerical analysis, and it discovered that the material's fatigue resistance can be increased at higher temperatures [32]. Using experimental tests and numerical analysis, the current study aims to investigate the effect of Laser surface treatment on the crack growth of AL-6061 Alloy under impact dynamic load. Under two types of fixations: Simply-Free-Simply-Free (SFSF) and Clamped-Free-Clamped-Free (CFCF) with a crack length of 5 mm and different aspect ratios of 1:1, 1:1.5, and 1: 2. The plate had previously been exposed to a 500-watt laser beam. This finding is of great significance as 6061-T6 aluminum plates are extensively used in airplane constructions and other structures. It helps to estimate the duration it will take for a crack to initiate and eventually lead to failure.

2. Material and Methods

The study utilized a 2mm-thick aluminum plate, 6061-T6, produced by Shandong International Ltd. [33]. Specifications are listed in Tables 1 to 3, cut into three sizes: 80mm x 80mm, 80mm x 120mm, and 80mm x 160mm. These sizes had aspect ratios (B/A) of 1:1, 1:1.5, and 1:2 respectively. To study the initial stages and propagation of a dynamic crack in an aluminum plate, a crack measuring 0.08 mm width and 5 mm long was created using a fiber laser machine. The crack was made in the center of the plate at a 0o angle of inclination, as illustrated in Figure 1. An electromechanical impact device shown in Figures 2-a, and b has been utilized for testing purposes. The device is composed of a motor that is connected to the gearbox, which helps to reduce the number of impacts. The lever attached

to raise the impact shift to a height of 60 mm. To determine the number of cycles required, the device has a sensor that calculates the number of cycles that are limited through the control board. The steel frame of the device permits various methods of installing plate edges, such as simply supporting the plate Simply-Free-Simply-Free (SFSF) or Clamp-Free-Clamp-Free (CFCF), based on the test that needs to be conducted. The impactor, weighing 1.5 kg, was placed perpendicularly to the crack area in the plate with a 6 mm diameter and struck at a rate of 20 impacts per minute. The Automatic Digital Crack Width Tester, CK102, is a precision tool used to measure and detect crack length and width as shown in Figure 3. The surface of the samples was treated using laser using a Remax fiber laser machine at a speed of 16 mm/s, 500 watts, 5 kHz, the laser beam line width was 0.03 mm and the distance in between the laser beam path was 0.5 mm.

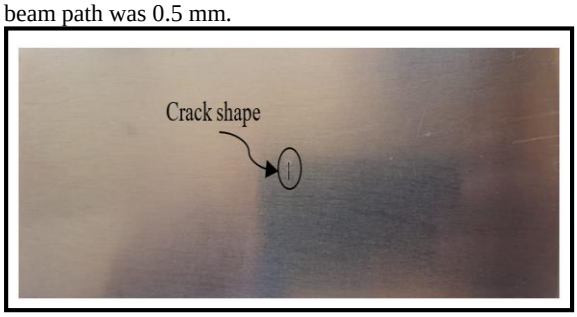

Figure 1: The crack shape in the AL-6061 plate

Table 1: Chemical composition of Aluminum alloy 6061-T6 [34]

Si%	Fe%	Cu%	Mn %	Mg%	Cr%	Zn%	Ti%	Other
0.74	0.42	0.22	0.07	1.04	0.12	0.04	0.04	0.1

Table 2: Mechanical properties of Aluminum alloy 6061-T6 [34]

Elastic modulus (GPa)	Passion ratio	Ultimate tensile strengths MPa	Tensile yield strengths MPa
68.9	0.33	310	276

Table 3: Thermal properties of Aluminum alloy 6061-T6[34]

AL-alloys	Thermal conductivity W/m · °C	Coefficient of thermal expansion (1/C)	specific heat capacity KJ/KG.K	Density Kg/m^3
6061-T6	167	23.6*10E-6	0.896	2700

3. Methodology

3.1. The impact-loading force

Using the work-energy principle [35], the impactor's velocity can be described as follows:

PE = KE (1)

Where PE is a potential energy and KE is a kinetic energy [35].

$$mgH = \frac{1}{2}mV^2 \quad (2)$$

Where, m is impactor mass (kg), g is gravitational acceleration (m/sec^2), H height of impactor and V is the velocity of impactor (m/sec), [35]

$$V = \sqrt{2gH} \quad (3)$$

Using the work-energy (We) principle from initial velocity V_{intial} and final velocity V_{final} [35]:

$$\text{We} = \frac{1}{2}mV_{final}^2 - \frac{1}{2}mV_{inital}^2 \quad (4)$$

$$V_{inital} = 0 \ , \ V_{final} = V \quad (5)$$

$$\text{We} = \frac{1}{2}mV^2 \quad (6)$$

From equation (6) the force of impact loading [35]:

$$F_{impct} = 2\text{We}/\text{H} \quad (7)$$

3.2. The impact loading force with time relation

As shown in Figure 4, that describe the impactor moves down from its position to impact the plate surface with a force equal to F_{impct}. It then takes t (sec) time to return to its original position.

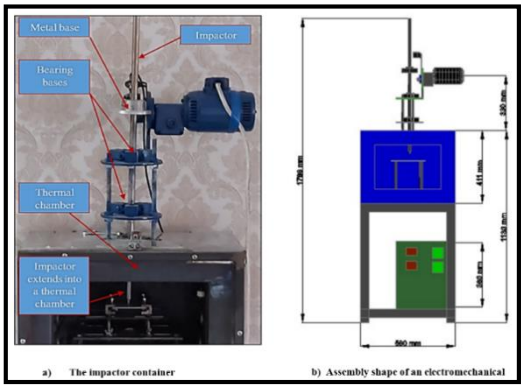

Figure 2-a, and b: The impactor electromechanical device

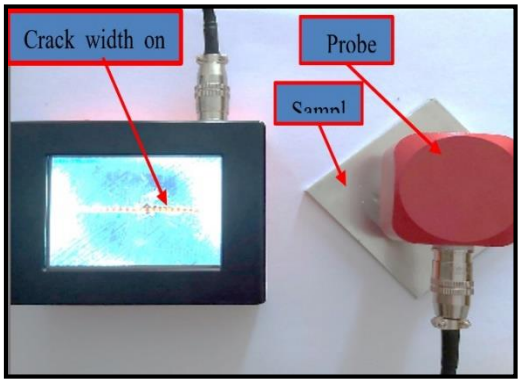

Figure 3: The automatic digital crack width tester

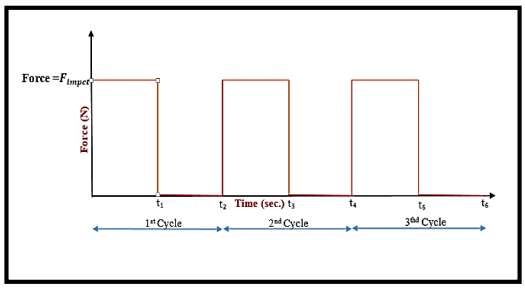

Figure 4: The cycle of the impact force with the time

  - Volume 18, Number 3 (ISSN 1995-6665)

To solve the problem of representing periodic functions effectively, a mathematical model utilizing the Fourier series method was employed [36].

$$F(x,y,t_i) = \frac{a_o}{2} + \sum_{n=1}^{N}\left[a_n\cos\left(\frac{n\pi t}{L}\right) + b_n\sin\left(\frac{n\pi t}{L}\right)\right] \quad (8)$$

Where: a_o, a_n, and bn are periodic function over (–L, L), L is one period time Cycling force of impact loading for one periodic, as a function of time (t) in (sec). The study adopts a specific impact wave at a height of 60 mm, and the device can be reset at different heights.

$$F(x,y,t_i) = \begin{cases} F_{impct} & 0 \le t \le t_1 \\ 0 & t_1 < t \le t_2 \end{cases} \quad (9)$$

To generate the final equation (10), the estimated values for equations for those values in as in equation 10:

$$F(x,y,t_i) = \frac{1}{2L}\int_{-L}^{L} T.\,dt + \sum_{n=1}^{N}\left[\begin{matrix}\frac{1}{L}\int_{-L}^{L} T\cos\left(\frac{n\pi t}{L}\right)dt\cos\left(\frac{n\pi t}{L}\right) + \\ \frac{1}{L}\int_{-L}^{L} T\sin\left(\frac{n\pi t}{L}\right)dt\sin\left(\frac{n\pi t}{L}\right)\end{matrix}\right] \quad (10)$$

3.3. The governing equation

The equation for calculating deflection in Cartesian coordinates takes into account the impact load F. Levy's solution provides formulas for plates that are clamped on both ends or simply supported on one side and free on the other. These formulas are used to determine the governing equation for plates under impact load [36].

$$D\left(\frac{\partial^4 w}{\partial x^4} + 2\frac{\partial^4 w}{\partial x^2\,\partial y^2} + \frac{\partial^4 w}{\partial y^4}\right) + m_2\frac{\partial^2 w}{\partial t^2} = F(x,y,t_i) \quad (11)$$

Where:-

$$D = \frac{E_2 h^3}{12(1-\nu_2^2)} \quad (12)$$

D is cylindrical rigidity of plate, h plate thickness, E_2, υ_2 are the young's modules and Poisson's ratio of plate respectively.

The initial condition of the problem is:-

$w = 0$ and $\frac{\partial w}{\partial t} = 0$ at $t = 0$

By the initial condition will get equation [36]:

$$\frac{\partial^4 w}{\partial x^4} + 2\frac{\partial^4 w}{\partial x^2\,\partial y^2} + \frac{\partial^4 w}{\partial y^4} = \frac{F(x,y,t_i)}{D} \quad (13)$$

The total solution for deflection w includes both the homogeneous solution for deflection, represented by w_h, and the particular solution for deflection, represented by w_p[36]:-

$$w = w_h + w_p \quad (14)$$

Total solution will be as in reference [36]: -

$$w_h = \sum_{m=1}^{\infty}[C_1\sinh\alpha_m y + C_2\cosh\alpha_m y + \alpha_m y(C_3\sinh\alpha_m y + C_4\cosh\alpha_m y)]\sin\alpha_m x \quad (15)$$

Where, C1, C2 for symmetric plate equal to zero, and late ($\alpha_m = \frac{m\pi}{A}$)

$$w_h = \sum_{m=1}^{\infty}[C_2\cosh\alpha_m y + \alpha_m y(C_3\sinh\alpha_m y)]\sin\alpha_m x \quad (16)$$

$$w_p = \frac{F(t_i)A^4}{\pi^4 m^4 D}.\sin\alpha_m x \quad (17)$$

3.4. Boundary Conditions

In Figure 5, the plate dimensions are displayed along with the axes' directions and the boundary conditions for the plate with crack orientation. Consider a plate that is two edges simply support (SFSF) at two points, x=0 and x=A, has two free edges on opposite sides, y=-B/2 and y=B/2 [37,38].

At: $y = B/2$ at any x and $\frac{\partial^2 w}{\partial y^2} = 0$

$$C_2\cosh\beta_m + C_3(\beta_m\sinh\beta_m + 2\cosh\beta_m) = 0 \quad (18)$$

At: $y = \frac{B}{2}$ at any $x and \frac{\partial^3 w}{\partial y^3} = 0$

$$C_2\sinh\beta_m + C_3(\beta_m\cosh\beta_m + 3\sinh\beta_m) = 0 \quad (19)$$

From equation (18 and 19) get[37,38]:

$$C_2 = 0 \quad (20)$$

$$C_3 = 0 \quad (21)$$

Consider a plate that has its edges clamped at x = 0 and x = A, while being free supported at the opposite edges y = 0 and y = B , [37,38].

At: y = B/2 at x = 0 and x = A, w = 0

$$\frac{F(t_i)A^4}{\pi^4 m^4 D} + C_2\cosh\beta_m + C_3\beta_m\sinh\beta_m = 0 \quad (22)$$

Where: $\beta_m = \frac{m.\pi.B}{2A}$

At: $y = \frac{B}{2}$ at $x = 0$ or $x = A$, $\frac{\partial w}{\partial y} = 0$

$$C_2\sinh\beta_m + C_3(\beta_m.\cosh\beta_m + \sinh\beta_m) = 0 \quad (23)$$

From equations (22 and 23) get[37,38]:

$$C_2 = \frac{-F(t_i)A^4}{\pi^4 m^4 D}\cdot\frac{(1+\beta_m\coth\beta_m)}{\beta_m\,\mathrm{csch}\,\beta_m + \cosh\beta_m} \quad (24)$$

$$C_3 = \frac{F(t_i)A^4}{\pi^4 m^4 D}\cdot\frac{1}{\beta_m\,\mathrm{csch}\,\beta_m + \cosh\beta_m} \quad (25)$$

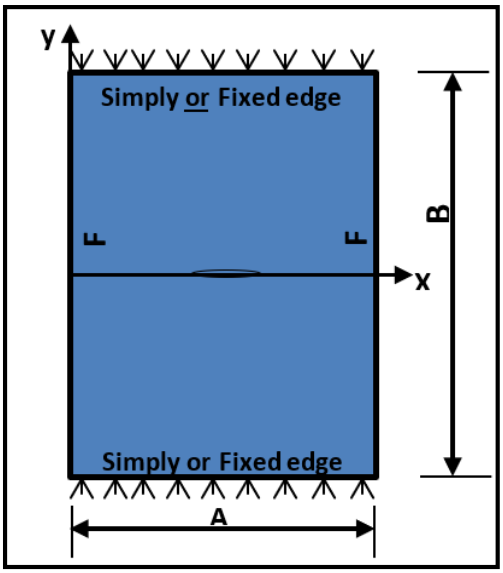

Figure 5: Location of clamping boundary condition of SFSF and CFCF

4. Numerical Analysis

4.1. Three-dimensional fracture modeling

By using quadratic elements, a three-dimensional model 3D was created to analyze a plate with a central crack. The mechanical and thermal properties of the plate's material, as

well as the stresses caused by the impact load, were defined, to determine the impact area and establish all the necessary initial conditions such as the plate's dimensions, crack length, crack angle, and installation method. As shown in Figures 6 and 7.The model consists of SOLID 187 quadratic elements, each of size 1 mm, of type 10-nodded tetrahedron elements.

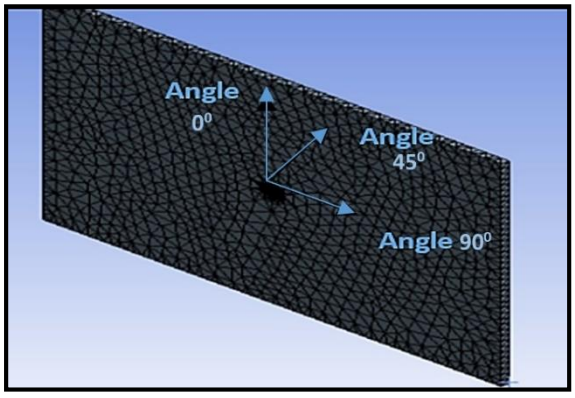

Figure 6: 3D meshing elements of a plate with a crack

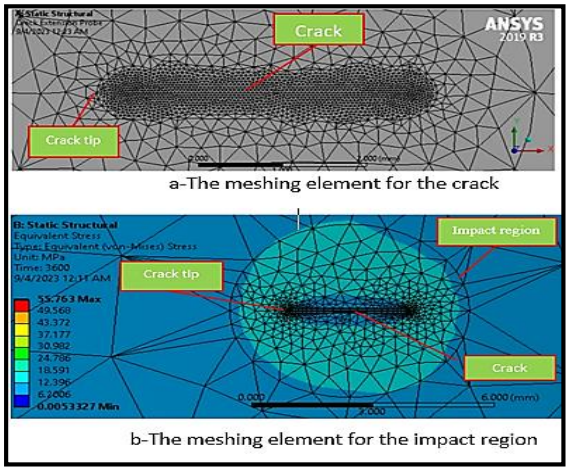

Figure 7: 3D meshing elements for crack

4.2. Boundary conditions

4.2.1. Apply impact stress

The purpose of the static model is to analyze the force of impact on the sample surface based on the electromechanical device's impact specifications, such as the weight of the impactor, the distance between the impactor and the sample surface, and the diameter of the impactor. The model simulated the impact stress caused by the force of the impactor on the

plate. The contact surface area between the impactor and the plate was defined, and the impactor was accurately configured with all its necessary data and the applied load function as shown in Figure 8. The outputs obtained from the first model were then used as inputs for the second model. The study examined the behavior of a 6061-aluminum plate that was Simply-Free-Simply-Free (SFSF) and Clamp-Free-Clamp-Free (CFCF). The dynamic load was applied to the plate in a specific location and direction. Figure 8 displays the model of the boundary conditions for the SFSF plate.

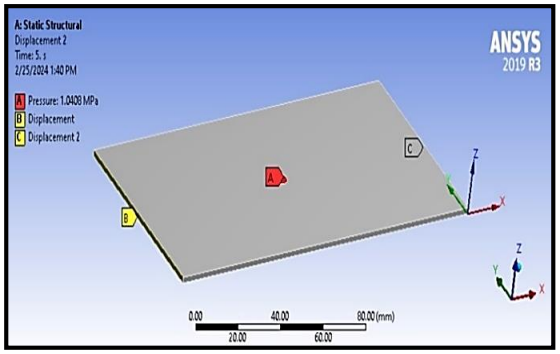

Figure 8: Model of the boundary conditions SFSF plate

4.2.2. Smart crack growth

At each solution step, SMART automatically updates the mesh of crack geometry that changes due to crack growth. This is different from the extended finite element method (XFEM). XFEM which uses the enrichment (segmentation) region. Figure9shows the final model built using SMART to calculate the growth of the crack after constructing models based on the output of each. A simulation model was built using ANSAS 19.0-R3 software to demonstrate the effect of the laser beam on the surface of the sample to determine the residual stresses generated in the aluminum plate. Since the laser beam is a beam of power that is transformed into heat on the surface of the sample in a regular manner and with a specific and controlled power, the heat flow characteristic was used to simulate the influence of the laser with a power of 500 watts, at a speed that simulates the speed of the laser machine in experimental tests. Figure 10 shows the effect of a laser beam fixed on both sides that has a length of 80 mm and free on both edges with a length of 160 mm.

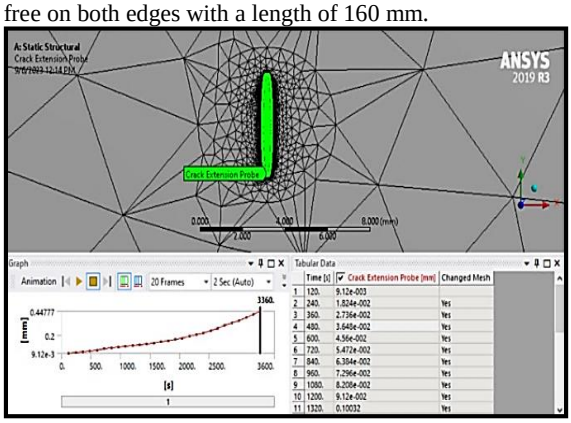

Figure 9: Model of smart crack growth under dynamic load

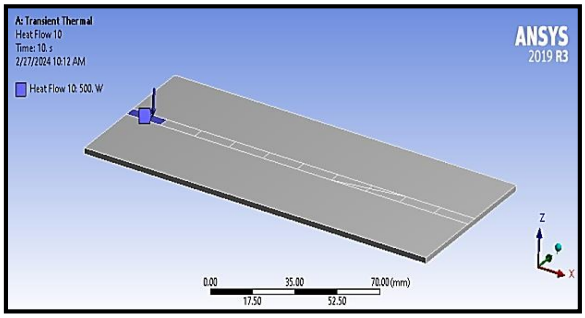

Figure 10: Simulation of the path of the laser beam on the surface of an aluminum plate

5. Results and Discussion

5.1. The effect of Laser beam

The results of an experimental and numerical indicate a significant influence of laser surface treatment on the mechanical behavior of crack propagation. Specifically, the Tp and Nip values estimated before crack propagation shows a noticeable effect. This observation suggests that laser surface treatment may have a significant impact on the mechanical behavior of materials under specific testing conditions. The following analysis presents the experimental outcomes and numerical results obtained for a sample of Al 6061-T6 with aspect ratio 1:2, clamped at two edges, with the other two edges being free, a crack angle of 0 degrees, and a length of 5 mm. The experimental results indicate that the initiation of crack growth commenced at a time of 93861 seconds and approximately 31287 impacts. On the other hand, the numerical results indicated that the initiation of crack growth began at a time of 93321 seconds and approximately 31107 impacts. The maximum percentage difference in the estimated Tp, Nip between the experimental and numerical results about 3.1%. Furthermore, the numerical results also recorded an increase of 36% and an increase of 37% for the experimental results compared to those estimated for the same sample specifications without laser surface treatment as shown in Figure 11. In Figure 12, a comparison between the experimental and numerical outcomes for an aluminum plate was presented. The plate is clamped at two edges and free on the other two edges. It has a 5mm long crack at an angle of 0º, which was not exposed to the laser beam. The practical results showed that the crack required approximately 19,663 impacts at a rate of 20 impacts per minute to begin growing, indicating that it took around 19,711 impacts for the crack to initiate in the sample. On the other hand, the numerical results.

The results of laser surface treatment were found to be noticeable, despite variations in the sample clamping methods employed. This finding can be attributed to the effects of laser beam power on the mechanical properties of the sample surface microstructure which is clean and controllable power. These results suggest that laser surface treatment can be a viable option for enhancing the mechanical properties of treated samples. The outcomes of the laser surface treatment were remarkable and exhibited a noticeable difference despite variations in the clamping techniques employed. The experimental data for a sample of Al 6061- T6 with aspect ratio 1:2, supported at two edges, and free at the remaining two edges (SFSF), with a 0o crack angle and a length of 5 mm, is presented. The experimental results showed that the crack growth started at around 47,654 impacts, while the numerical results indicated that the crack started at approximately 47,394 impacts. The maximum difference in the estimated percentage of Tp and Nip between the experimental and numerical results was about 3%. The numerical results also showed a 28% and 29% increase in the experimental results compared to those estimated for the same sample specifications without laser surface treatment, as indicated in Figure 13. The data shown in Figure 14 pertains to an aluminum plate that is simply supported at two edges while the other two edges are free has a crack with a length of 5 mm. The plate was not exposed to any laser beams and the crack length was 5 mm, inclined at 0º. According to Figure 14, the experimental results indicate that it takes 33,957 impacts for crack growth to begin. On the other hand, the numerical results suggest that it takes 33,917 impacts for crack growth to start. The sample was subjected to a rate of 20 impacts per minute.

In general, based on a comparison of the results shown in Figures 11 to 14, it can be concluded that the laser beam increased the plate's resistance to crack growth. Additionally, the number of beats needed for the crack to grow was lower in the plate with the CFCF type of clamping than in the plate with the SFSF type of clamping due to the influence of the clamping conditions as well as the effect of the laser beam.

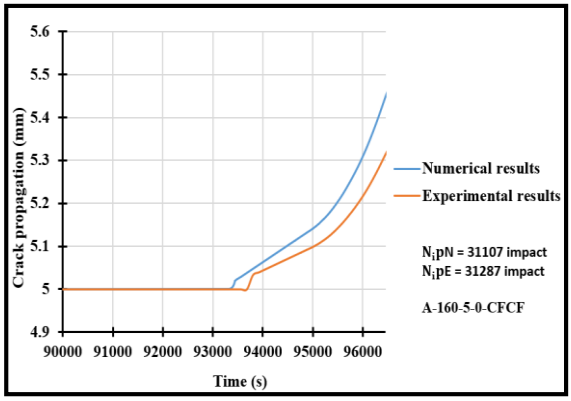

Figure 11: The crack propagation with time estimated numerically, and experimentally in A-160-5-0-CFCF with laser surface treatment

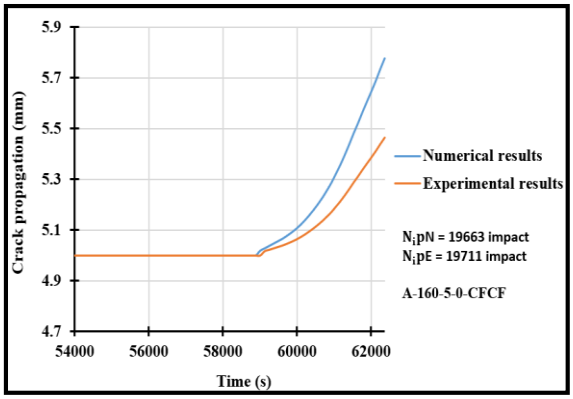

Figure 12: The crack propagation with time estimated numerically, and experimentally in A-160-5-0-CFCF without laser surface treatment

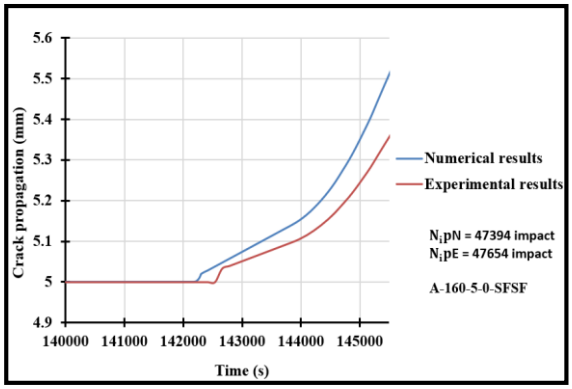

Figure 13: The crack propagation with time estimated numerically, and experimentally in A-160-5-0-SFSFwith laser surface treatment

5.2. Effect of the aspect ratio of the plate

Figure 15, shows the results of an experiment conducted on a sample of 6061 aluminum plate. The sample had dimensions of 80 mm * 160 mm and was supported from two edges while the other two edges were free. The figure displays the experimental, and numerical results of the sample. The results of the experimental and numerical analysis of dynamic crack growth in a simple support plate with two edges fixed and the other two free, having dimensions of 80 mm * 160 mm. The plate was subjected to a laser beam with a power of 500 watts. The experimental findings indicated that the crack began to grow after 56157 impacts, while the numerical results required 55897 impacts for the crack to start growing at a rate of 20 impacts per minute. According to the experimental data, the increase in the ratio of impacts required to initiate crack growth was 31.8% compared with a plate that has the same boundary condition without exposure to the laser beam. Similarly, the percentage of increase in the ratio of impacts due to the influence of the laser beam on the plate was 32%. Figure 16 displays experimental and numerical results on the effect of a laser beam on an aluminum plate measuring 120 mm * 160 mm. The plate was supported from two edges and free from the other two. The experiment exposed the plate to 500 watts of laser power. The study aimed to evaluate the influence of the laser beam's intensity and its interaction with the plate's material properties. The results display a significant interaction between the laser power and the crack growth rate. Furthermore, the study highlights the importance of considering the laser's power level while investigating the dynamic crack growth phenomenon. Experimental and numerical results show the effect of a laser beam on dynamic crack growth in a 6061-aluminum plate at a rate of 20 impacts per minute. When a plate is exposed to a laser beam with a power of 500 watts, it takes 52667 impacts for the crack to start growing. However, if the same plate is subjected to dynamic load, the stresses concentrate on the tips of the crack, and it requires 52407 impacts for the crack to begin to grow at its tips. These findings are based on both experimental and numerical data. After comparing the experimental and numerical results, it was observed that a plate with dimensions of 120 mm * 160 mm, which was previously exposed to a laser beam with a power of 500 watts, had 31.34% more impact than the one that was not exposed to the laser beam under the same boundary conditions. The experimental results showed an increase of 31.34% in the number of impacts, while the numerical results showed an increase of 31%.

Experimental and numerical results for an aluminum plate. The aluminum plate with dimensions 160 mm by 160 mm contains a crack with a length of 5 mm and a simple support of two edges and the other two edges are free, illustrated in Figure 17. The surface of the sample was exposed on both sides to a laser beam with a power of 500 watts. As a result of the effect of the laser beam, it was found that the number of impacts required for dynamic crack growth at a rate of 20 impacts per minute according to the results of the process increased by 28.74%, while the numerical results showed an increase of 28.44% compared to the sample without exposure to the laser beam. Increasing the rate of impact required for the initial crack growth at the crack tips indicates an improvement in the resistance to crack growth in samples that are exposed to the laser beam. The improvement in resistance to crack growth is an indicator of enhancing the mechanical properties of the aluminum plate without any additives. It is considered an important value in using lasers to improve the resistance of metals to crack growth and failure, and it has an impressive economic feasibility because the process is carried out without any additives.

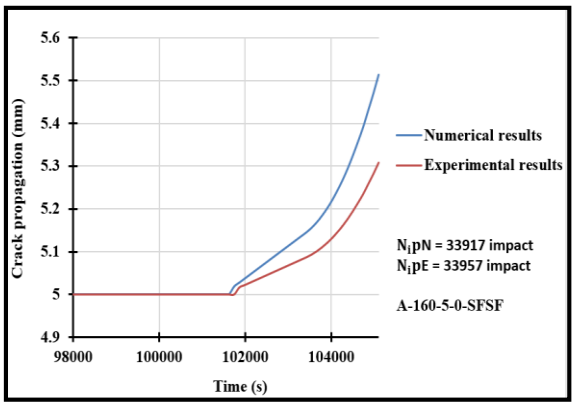

Figure 14: The crack propagation with time estimated numerically, and experimentally in A-160-5-0-SFSF without laser surface treatment

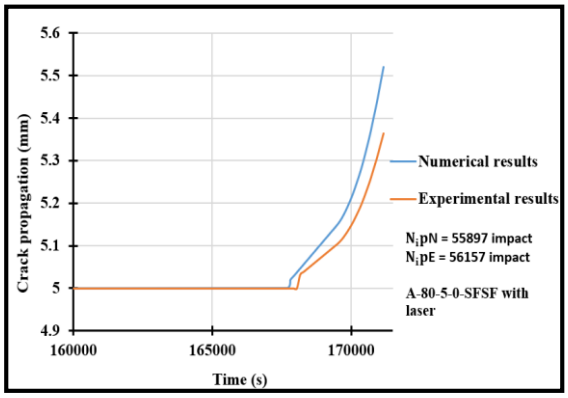

Figure 15: The crack propagation with time estimated numerically, and experimentally in 80-5-0-SFSF with exposure to 500-watt laser beam

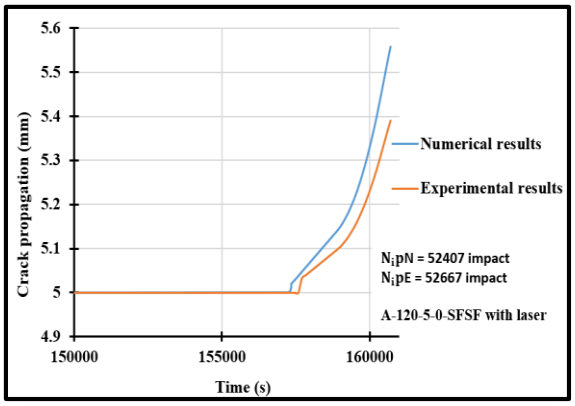

Figure 16: The crack propagation with time estimated numerically, and experimentallyin 120-5-0-SFSF with exposure to 500-watt laser beam

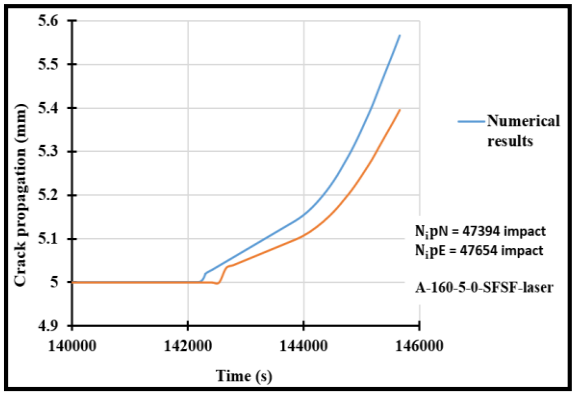

Figure 17: The crack propagation with time estimated, numerically, and experimentally in160-5-0-SFSF with exposure to 500-watt laser beam

In general, the results indicated a decrease in the number of beats required to start the initial crack propagation when comparing the results in Figures 15, 16, and 17 at various aspect ratios of 1:1, 1:1.5, and 1:2 under the same SFSF clamping settings. According to the experimental and numerical results, the study found that the number of beats required for crack growth at the aspect ratio of 1:1 was 31.8% and 32%, while it was 31.34% and 31% at the aspect ratio of 1:1.5, furthermore, it was 28.74% and 28.44% at the aspect ratio of 1:2, respectively.

5.3. Numerical Results

A three-dimensional numerical analysis was conducted on a plate that was subjected to a laser power of 500 watts. The CFCF installation shown in Figure 18 reveals the distribution of equivalent stress that is concentrated in the area where the impactor hits the plate. Under the influence of the dynamic impact load with an aspect ratio of 1:1, the maximum value of

equivalent stress was found to be 31.45 MPa. While, for a plate with an aspect ratio of 1:1.5 under the same clamped conditions, Figure 19 shows that the maximum stress is 35.564 MPa. Furthermore, Figure 20 illustrates a plate with an aspect ratio of 1:2, where the maximum stress is concentrated at the two tips of the crack, with a maximum value of 44.327 MPa under the same clamped conditions.
The Von-Mises stress distribution on an aluminum plate shows stress concentration at the center of a laser beam, leading to thermal expansion causing maximum bending at the plate's midpoint. Analysis was conducted at 1.03 sec, 4.74 sec, and 9.47 sec during the laser beam's movement on the plate surface (see Figures 21-a, b, and c).

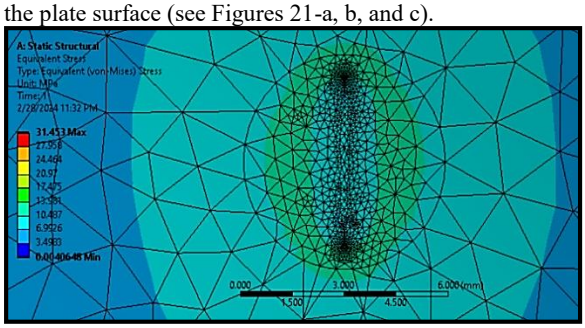

Figure 18: The Equivalent Von-Mises stress in the crack of 80-5-0-CFCF with exposure to 500-watt laser beam

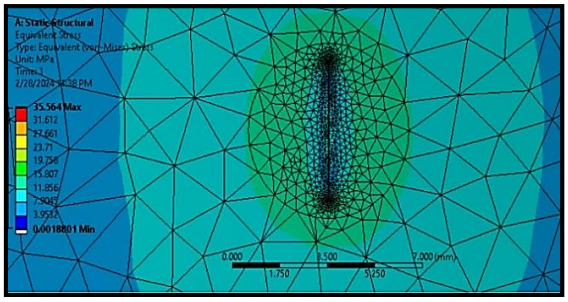

Figure 19: The Equivalent Von-Mises stress in the crack of 120-5-0- CFCF with exposure to 500-watt laser beam

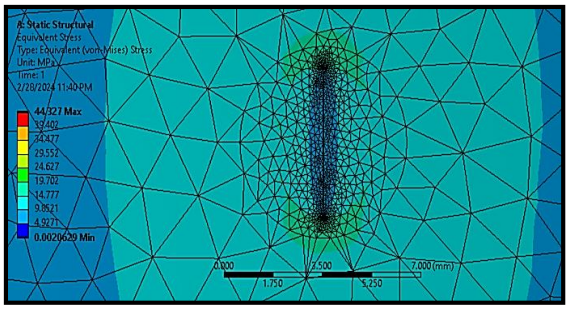

Figure 20: Contour of the Equivalent Von-Mises stress in the crack of 160-5-0- CFCF with exposure to 500-watt laser beam

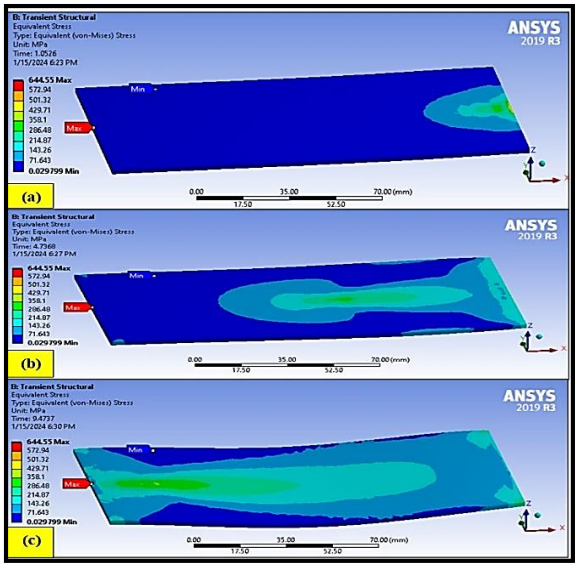

Figure 21-a,b, and c: Simulation of laser surface treatment at time of 1.026 sec, (b) at time of 4.737 sec, and (c) at time of 9.474 sec

In Figure 22, the distribution of strain along a crack varies with boundaries under dynamic load at 500 watts. Strain concentrates at crack tips, leading to crack growth. A numerical study on an 80 mm * 80 mm plate shows 12.25% higher equivalent strain in CFCF than SFSF plates. CFCF clamped plates are projected to have faster crack growth than SFSF plates under dynamic load. Numerical analysis revealed that on an 80mm x 80mm plate exposed to 500 watts of laser power and clamped by CFCF or SFSF, the highest equivalent stress occurs at the crack ends. The crack growth is expected at both ends. The stress rate from dynamic impact loading on a CFCF-clamped plate is 12.47% higher than that on an SFSF-clamped plate. The CFCF plate's highest stress is 16.367 MPa, while the SFSF plate reaches 16.093 MPa at both ends of a 5 mm crack.

Numerical analysis is crucial for understanding strain concentration, predicting crack growth, and identifying potential failure points in various industrial applications like aircraft fuselage structures and automobiles. It plays a vital role in developing effective strategies to prevent crack propagation in industrial settings.

Numerical analysis was performed on a 120mm x 80mm plate exposed to a 500-watt laser beam to study strain distribution. The study examined two clamping types, CFCF and SFSF, finding higher strain values at crack ends for both. CFCF had 3.23% higher average strain than SFSF, suggesting it may experience faster crack propagation. The CFCF plate showed lower strain at the crack middle, indicating better energy transfer, while SFSF exhibited greater curvature due to energy loss at the crack edges under dynamic loading.The distribution of the equivalent strain along the crack length of the sample types 120-5-0 SFSF and A-120-5-0 CFCF at each impact load with a laser power of 500 watts is shown in Figure 24.

The strain concentration at the tips of the crack led to an increase in the prediction of crack growth at those points. The results showed that the rate of difference in strain concentration was 3.23% when comparing the two types of installation: CFCF and SFSF.A comparison was made to analyze stress distribution along a crack in a plate subjected to a 500-watt laser beam, as shown in Figure 25. The plate, measuring 120 mm by 80 mm, was clamped using two different methods: CFCF and SFSF. Results indicated that the CFCF plate exhibited a 3.5% higher equivalent stress rate compared to the SFSF plate. This higher stress level in the CFCF plate was found to potentially lead to crack growth at the edges of the SFSF crack due to stress concentration. In contrast, the middle section of the CFCF crack experienced lower equivalent stress levels than the SFSF plate. Specifically, the CFCF clamping method resulted in a maximum stress of 14.237 MPa at the crack tip, while the SFSF clamping recorded 11.735 MPa, highlighting higher stress concentration in the CFCF clamping method.

The study compared equivalent strain distributions along a 5mm crack in a plate with dimensions 160mm by 80mm (aspect ratio 1:2) exposed to a 500-watt laser beam and dynamic impact load as shown in Figure 26. Two clamping methods, CFCF and SFSF, were assessed. Results indicated similar behavior for aspect ratios 1:1 and 1:1.5, with strains concentrated at crack tips. CFCF clamping had higher average equivalent strain by 1.51% and 31.53% higher strain at crack tips compared to SFSF. CFCF plates exhibited a wider range of strain changes than SFSF. The study highlighted the direct proportionality of equivalent strain to plate aspect ratio under dynamic impact loading. Plate aspect ratio (B/A) significantly influences plate response to dynamic impact loads, impacting material design for such applications. Figure 27 illustrates the distribution of equivalent stress in a plate under dynamic load with an aspect ratio (B/A) of 1:2 which was exposed to a laser beam at a power of 500 watts and subject to dynamic load. The plate was clamped by two methods: CFCF and SFSF. The study displayed that the stress is concentrated at the two tips of the crack of equivalent stress in the plate with an aspect ratio of 1:2 is similar behavior to that of the plates that have aspect ratios of 1:1 and 1:1.5, but with a higher range of equivalent stress. So, the study found that the equivalent stress rate of the CFCF plate was 31.59% higher than that of the SFSF plate.

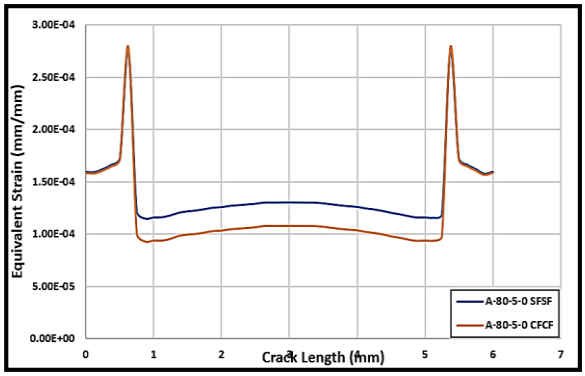

Figure 22: Compare the distribution of the equivalent Strain along the crack length of the sample type 80-5-0 SFSF and A-80-5-0 CFCF at each impact load with laser power 500 watt

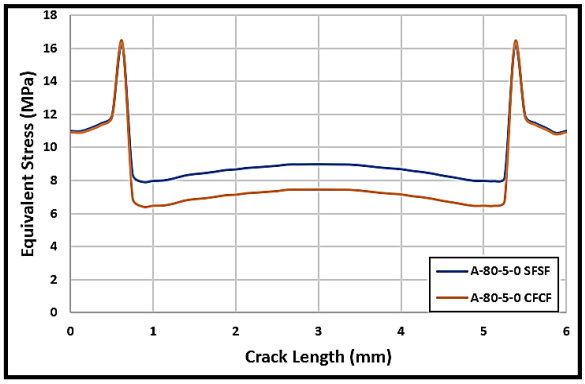

Figure23: Compare the distribution of the equivalent Stress along the crack length of the sample type 80-5-0 SFSF and A-80-5-0 CFCF at each impact load with laser power 500 watt

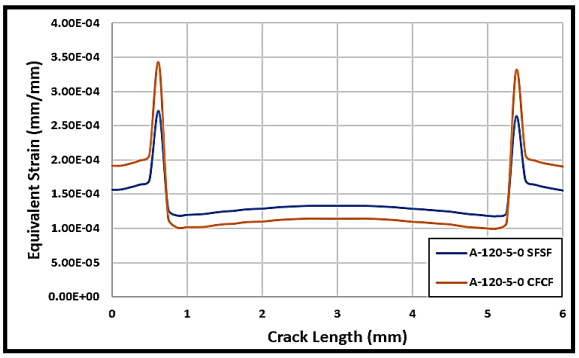

Figure24: Compare the distribution of the equivalent Strain along the crack length of the sample type 120-5-0 SFSF and A-120-5-0 CFCF at each impact load with laser power 500 watt

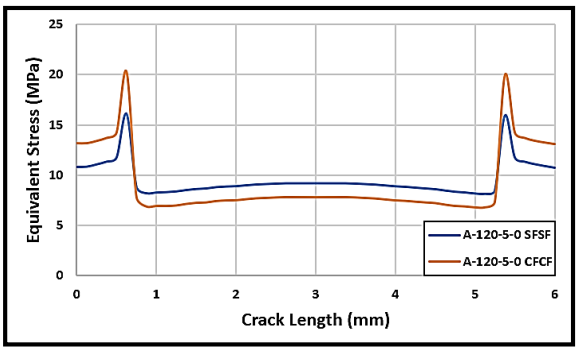

Figure25: Compare the distribution of the equivalent Stress along the crack length of the sample type 120-5-0 SFSF and A-120-5-0 CFCF at each impact load with laser power 500 watt

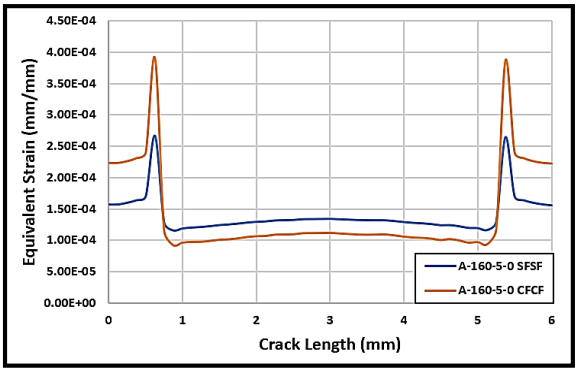

Figure 26: Compare the distribution of the equivalent strain along the crack length of the sample type 160-5-0 SFSF and A-160-5-0 CFCF at each impact load with laser power 500 watt

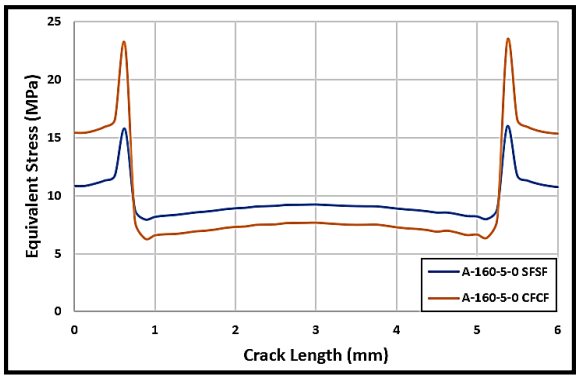

Figure 27: Compare the distribution of the equivalent stress along the crack length of the sample type 160-5-0 SFSF and A-160-5-0 CFCF at each impact load with laser power 500 watt

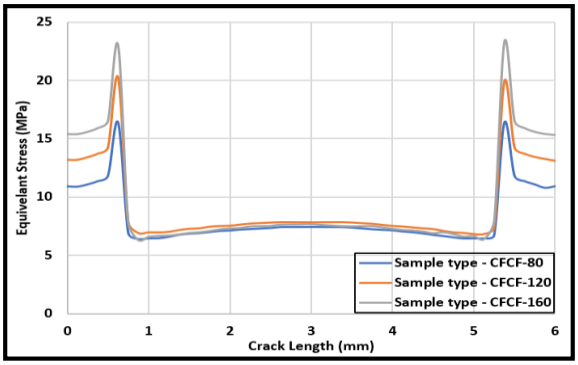

Figure 28: Compare the distribution of the equivalent stress along the crack length of sample type CFCF of different aspect ratio 1, 1.5, and 2 with laser power 500 watts

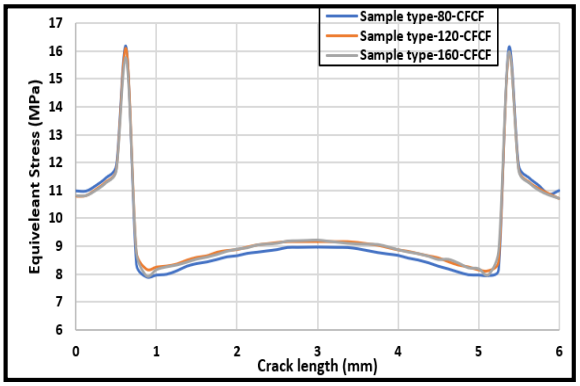

Figure 29: Compare the distribution of the equivalent stress along the crack length of sample type SFSF of different aspect ratio 1, 1.5, and 2 with laser power 500 watts

When comparing the effect of the aspect ratio on the equivalent stress rate at the type of CFCF clamping in the plate with an aspect ratio of 1:2 by 4.26% compared to a plate with an aspect ratio of 1:1.5, while it was higher by 10.59% compared to a plate with an aspect ratio of 1:1 as shown in Figure 28, while the effect of the aspect ratio on the equivalent stress rate at the type of SFSF clamping in the plate with an aspect ratio of 1:2 was at a rate of 0.12 % compared to a plate with an aspect ratio of 1:1.5, while it was higher by a rate of 1.4% compared to a plate with an aspect ratio of 1:1 as shown in Figure 29.

When a plate undergoes dynamic loading, it experiences bending and tensile stresses. Bending stress depends on metal properties and its ability to bend, while tensile stress in the plate at the edges is influenced by clamping type conditions. Clamping with CFCF type leads to more tensile stress and crack growth, whereas SFSF clamping converts impact stress to bending stress, reducing crack growth. CFCF-clamped plates show faster crack propagation than SFSF. Figure 30 shows the temperature distribution of a laser beam on an aluminum plate at various distances. The findings demonstrated the maximum aluminum plate's surface temperature varies between 289.44 C^{o} and 322.56 C^{o}. The microstructure and mechanical properties of the plate are influenced by the heat factor produced by the laser beam. As a result, pinpointing its ranges is crucial to creating an accurate description of the temperature conditions it was subjected to Sample. According to the results, the temperature is highest in the center of the laser beam and lowers in the surrounding area as a result of air cooling brought on by the aluminum plate's convection and the distance from the laser beam.

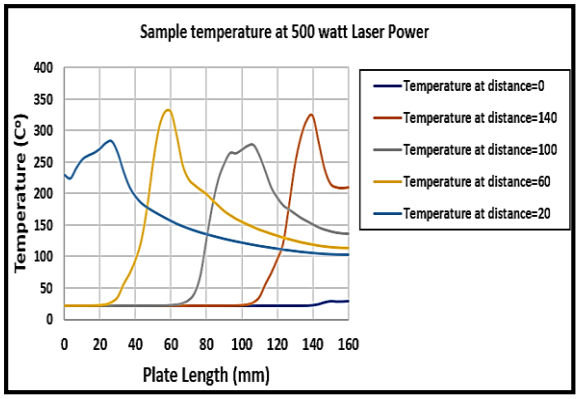

Figure30: The distribution of temperature (C°)along the sample type 160-5-0 CFCF

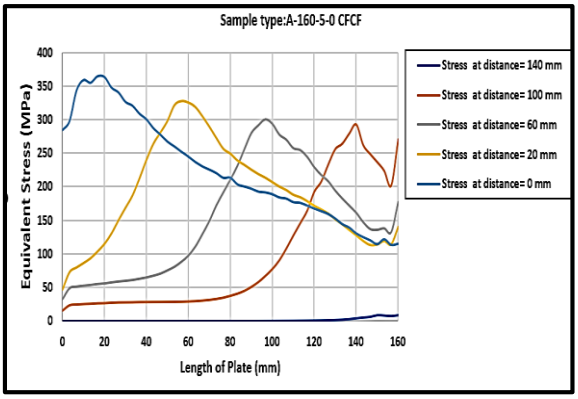

Figure 32: The distribution of the equivalent stress along of sample type 160-5-0 CFCF during laser beam 500-watt pass

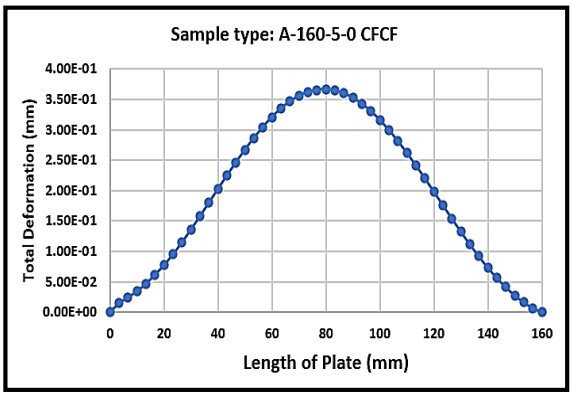

Figure 31: The distribution of total deformation along the sample type160-5-0 CFCF at 500 watts.

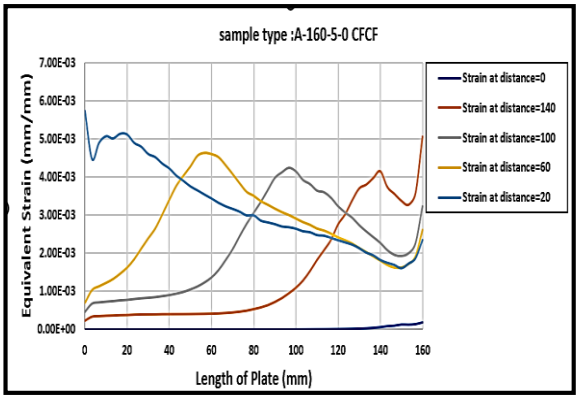

Figure 33: The distribution of the equivalent strain along of sample type 160-5-0 CFCF during laser beam 500-watt pass

As demonstrated in Figure 32, residual stresses are created when a 500-watt laser beam hits an aluminum plate with an aspect ratio of 2.0 and a clamping type of CFCF. These stresses have an impact on the sample's hardening and strengthen its resistance to fracture propagation. At 0 mm, 20 mm, 60 mm, 100 mm, and 140 mm, the maximum equivalent stress generated by the laser beam was 363.16 MPa, 325.56 MPa, 293.87 MPa, 292.85 MPa, and 282.85 MPa, respectively. For the CFCF mounting type, Figure 33 displays the distribution of the equivalent strain that results from a 500-watt laser beam passing through the centre path of the aluminum plate at distances of 20 mm, 60 mm, 100 mm, and 140 mm, 0 mm, or 160 mm. The findings indicated that the maximum equivalent strain values were 0.0051, 0.0046, 0.0041, 0.00415, and 0.00017 at distances of 20 mm, 60 mm, 100 mm, and 140 mm, 0 mm, or 160 mm, respectively.

The overall deformation strain of a plate subjected to a laser beam's effect is illustrated in Figure 34 when the aspect ratio of the SFSF installation type is 2.0. The results showed that the maximum total deformation strain resulting from the dynamic impact load is at the ends of the plate, while its value is lowest in the middle of the aluminum plate. The maximum total deformation strain at the edges was 98.68% greater than in the middle of the plate, which is the result of the effect of the installation conditions of the SFSF type. The equivalent stress generated by the laser beam for an SFSF-type aluminum plate with an aspect ratio of 2.0 at distances of 20 mm, 60 mm, 100 mm, 140 mm and 0 mm or 160 mm is shown in Figure 35. The results showed that the equivalent stress was 189.78 MPa, 296.62 MPa, 250.03 MPa, 199.12 MPa, and 7.7051 MPa when the beam passed at the following distances: 20 mm, 60 mm, 100 mm, 140 mm, and 0 mm or 160 mm. Figure 36 shows the equivalent strain created by the laser beam for an SFSF-type aluminum plate with an aspect ratio of 2.0 at distances of 20 mm, 60 mm, 100 mm, 140 mm, and 0 mm or 160 mm. The results showed that the equivalent strain was 0.00269, 0.00421, 0.00353, 0.00285, and 0.000137 mm/mm when the beam passed at the following distances 20 mm, 60 mm, 100 mm, 140 mm, and 0 mm or 160 mm respectively.

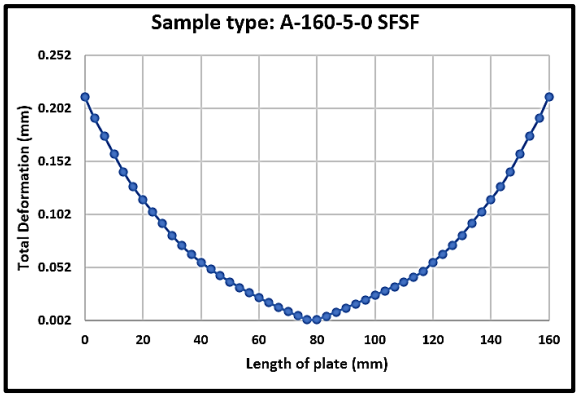

Figure 34: The distribution of total deformation along the sample type 160-5-0 SFSF at 500 watts

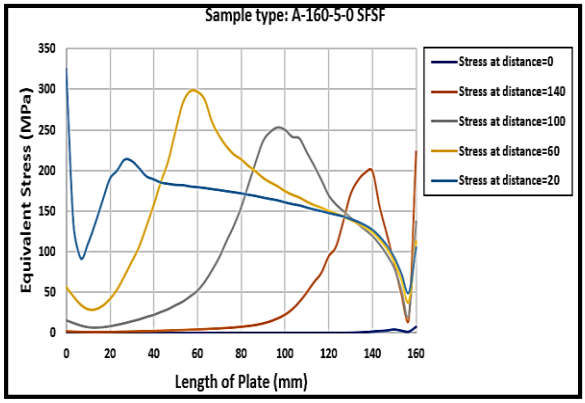

Figure 35: The distribution of the equivalent stress along of sample type 160-5-0 SFSF during laser beam 500-watt pass

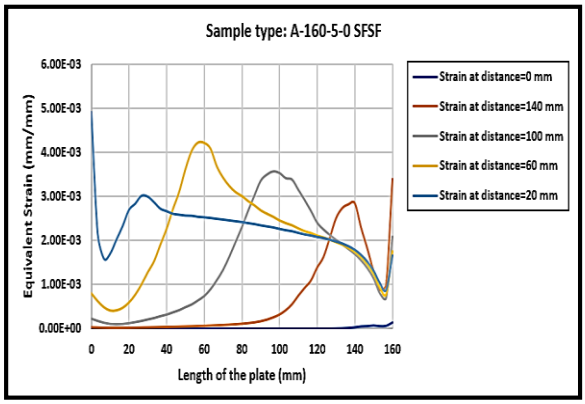

Figure 36: The distribution of the equivalent strain along of sample type 160-5-0 SFSF during laser beam 500-watt pass

When the effects of the laser beam at the two different clamping types were compared in Figures 32 with 35 and Figures 33 with 36, it became clear that the aluminum plate with the clamping type CFCF had higher equivalent strain and stress than the plate with the clamping type SFSF. This is because the heat produced by the laser beam's power causes thermal expansion, which pushes toward the ends fixed with the clamping type CFCF and increases the stress generated on the plate; this effect is less pronounced for the plate with the clamping type SFSF.

5.4. The Microstructure SEM Images

The scanning electron microscope (SEM) images obtained at 20 kV with an accuracy of 108.3 µm and an accuracy of 107.7 µm were used to capture high-accuracy images of the plate surface microstructure to analyze the effect of the laser beam on the microstructure of the samples before and after the laser surface treatment, presented in Figure 37. The study investigated the effect of the laser beam on the microstructure of the surface of the aluminum plate to understand the reasons that led to enhanced resistance to crack growth on the plate exposed to the laser beam. The SEM images taken at an accuracy of 107.7 micrometers of the microstructure of the surface of the aluminum sample before it was exposed to the laser beam showed that the surface was smooth, as shown in Figure 37-a, while the SEM image of the microstructure of the surface of the aluminum plate after the laser beam at an accuracy of 108.3 micrometers showed increased the surface roughness resulting from a change in Microstructure due to the heat generated by the laser beam. The change in the shape of the microstructure due to the heat of the laser beam generated residual stresses in the plate, in addition to raising the hardness of the surface of the aluminum plate, which contributed to increasing its resistance to crack growth and improving its properties in resisting failure. Therefore, the improvement in resistance to failure was the reason for the increase in time and impact number required to begin the initial dynamic crack growth at both crack tips.

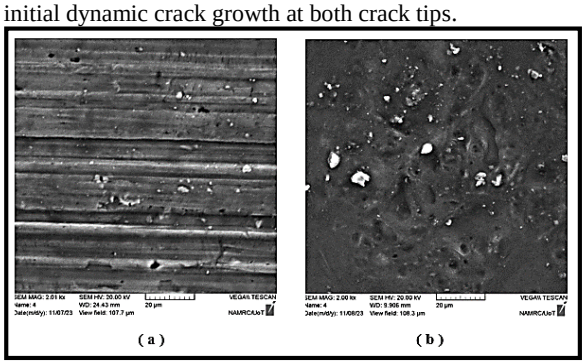

Figure 37-a and b: (a)-SEM images of 6061-T6 before laser surface treatment(b)-SEM images of 6061-T6 after laser surface treatment

6. Conclusions

The study investigated the impact of a laser beam on the growth of cracks in an aluminum plate of AL-6061 at different aspect ratios of 1:1, 1:1.5, and 1:2. The plate has a crack length of 5 mm and was supported by two clamping types CFCF and SFSF. The study aimed to determine the time it takes for the cracks to propagate under the influence of a dynamic load after being exposed to 500-watt laser energy. This is important because the 6061-T6 alloy is commonly used in the aerospace, automotive, and construction industries to make structural components. The study concluded that:

- The study concluded, based on experimental tests and numerical analysis, that Tp and Nip increase when the plate is exposed to a laser beam under the same installation conditions and aspect ratio. The study found that the number of impacts (Nip) required for crack growth (Tp) according to the numerical results increased by 36% while increased by 37% according to the experimental results of the clamping type CFCF. When the type of clamping was SFSF, it was found that the number of impacts required to initiate the growth of the

initial crack (Nip) of a plate that was exposed to a laser beam increased in the experimental results by 28%, while it increased by 29% according to the numerical results. It appears that the laser beam is an effective factor in improving the resistance of the plate to crack growth, which opens the way for research into its use in various fields to develop its use in industrial and applied fields.

- The present study explains the stress distribution along the length of a crack and its implications for fracture propagation. Specifically, the largest stress value was identified at the two tips of the crack, with the CFCF-type clamping at aspect ratio 1:1 exhibiting a 12.47% greater stress concentration in comparison to the SFSF-type clamping. Consequently, the fracture in the CFCF clamping grew at a faster rate than initially anticipated, which has critical implications for industries such as aviation, automobiles, and structures where crack formation and failure may occur. These findings underscore the need for careful consideration in the selection of clamping types and fixation techniques in the design and maintenance of structures exposed to cyclic loading.
- The study found that at an aspect ratio of 1:1.5, the CFCF clamping type had an equivalent stress rate 1.5% higher than the SFSF clamping type. Moreover, at the ends of the crack, the equivalent stress was 31.53% greater when compared to the SFSF clamping type. This conclusion has significant implications for the design and engineering of materials used in applications subjected to dynamic impact loads.
- When comparing the aspect ratio's effect on the equivalent stress rate at the CFCF clamping type in the plate, it was found that the aspect ratio of 1:2 resulted in a 4.26% increase in the stress rate compared to a plate with an aspect ratio of 1:1.5. In turn, it was higher by 10.59% compared to a plate with an aspect ratio of 1:1. However, the effect of the aspect ratio on the equivalent stress rate at the SFSF clamping type in the plate with an aspect ratio of 1:2 was only 0.12% compared to a plate with an aspect ratio of 1:1.5, and in turn was higher by 1.4% compared to a plate with an aspect ratio of 1:1.
- The study concluded that the temperature on the surface of the plate resulting from the laser beam at a power of 500 watts ranged between 289.44 C^o and 322.56 C^o, and it is considered an important indicator in the field of developing laser beam use in various to improve properties of product in industrial applications. Moreover, is an important research path in its use by advanced technologies.
- Based on the results, it has been found that the CFCF clamp type with an aspect ratio of 1:2 displays maximum total deformation strain at the center of the plate when the clamped plates are subjected to dynamic impact loading conditions. On the other hand, the SFSF clamp type behaves in an opposite manner due to the clamped boundary conditions.
- The SEM images, which were obtained with an accuracy of 107.7 and 108.3 micrometers, demonstrated how the laser beam affected the sample's surface. The power of the laser beam caused heat to be released into the sample's microstructure, which enhanced the material's resistance to crack growth. In contrast, the aluminum plate's surface, which was not exposed to the laser beam, appears smoother.

ACKNOWLEDGEMENTS

We would like to thank the University of Technology, especially the Electromechanical Engineering Department for their support in completing this work.

REFERENCES

[1] Oda, J., Murotsu, Y. Mechanical Design Engineering (I) Element & Design. Vol. 5., Baifukan, Tokyo, Japan; 2000.

[2] Gerlach, R., Siviour, C.R., Petrinic, N., Wiegand, J., Experimental Characterization and Constitutive Modelling Of RTM-6 Resin Under Impact Loading, Polymer, Vol. 49, 2008, pp.2728–2737.

[3] Dannemann, K.A., Chalivendra, V.B., Song, B., "Dynamic Behavior of Materials", Exp. Mech., Vol.52, 2012, pp.117–118.

[4] Yan Peng, Yang Liu, and Wei Zhang, "Analysis of Dynamic Response Behavior of Crack under Impact Stress Wave", Metals, Vol.11, Issue 1920, 2021, pp.1-16.

[5] ShaymaaMezaalMshattat, Hussein J Al-Alkawi, and Ahmed Hameed Reja, "Buckling at Elevated Temperature for (6061-T6) Aluminum Alloy Columns under Increasing Load", IICESAT Conference, College of Material Engineering, University of Babylon, Iraq, 2021.

[6] Giannella, V.; Sepe R., Citarella, R. "Fatigue Crack Propagation for an Aircraft Compressor Under Input Data Variability", Procedia Struct. Integr., Vol.41, 2022, pp. 298-304.

[7] Ahmad, S., Egilmez, M., Iqbal, M., Ibrahim, T., Khamis, M., Alnaser, A.S. , "Pulsed Laser Deposited Zeolite Coatings on Femtosecond Laser-Nanostructured Steel Meshes for Durable Superhydrophilic/Oleophobic Functionalities", Front. Chem., Vol. 9, No.1027, 2021, pp.1-12.

[8] Ali, A., Piatkowski, P., Nawaz, T., Ahmad, S., Ibrahim, T., Khamis M., Alnaser A.S., "A Two-Step Femtosecond Laser-Based Deposition of Robust Corrosion-Resistant Molybdenum Oxide Coating", Materials, Vol.16, No.909, 2023, pp.1-16.

[9] R N Hwayyin, A S Hammood, "Improving the Properties of Acrylic by Creating Crack Using Laser Beam". 1st International Conference on Petroleum Technology and Petrochemicals, IOP Conf. Series: Materials Science and Engineering 579, Baghdad, Iraq, 2019.

[10] Raed Naeem Hwayyin, Azhar Sabah Ameed, Ahmed Salman Hamood, "Study the Effect of the Shape of the Laser's Path on the Mechanical Properties of Acrylic Layer", Jordan Journal of Mechanical and Industrial Engineering, Vol.16, Issue 5, 2022, pp.333-341.

[11] Ahmad S., Egilmez, M., Kannan, A.M., Alnaser A., "Oxygen Evolution Reaction Enhancement of Copper Electrodes In Alkaline Medium Using Ultrafast Femtosecond Laser Structuring", Int. J. Hydrogen Energy Vol. 52, Part D, 2024, pp.2-13.

[12] Giannella, V., "Uncertainty Quantification in Fatigue Crack-Growth Predictions", Int. J. Fract. Vol. 235, 2022, pp.179–195.

[13] Giannella V., Amato D., Perrella M., "Stability of Cruciform Specimens for Fracture Tests Under Compression", Eng. Fract. Mech., Vol. 261, No.108247, 2022, https://doi.org/10.1016/j.engfracmech.2022.108247.

[14] E. Amsterdam, J.W.E. Wiegman, M. Nawijn, J. Th. M. De Hosson, "The Effect of Crack Length and Maximum Stress on The Fatigue Crack Growth Rates of Engineering Alloys", International Journal of Fatigue, Vol.161, 2022, pp.1-17.

[15] Xiangxiang Chen, Xudong Chen, Chan A., Cheng Y., Wang H., "A FDEM Parametric Investigation on the Impact Fracture of Monolithic Glass", Buildings, Vol.12, No.271, 2022, pp.1-20.

[16] Chen X., Luo T., Ooi E.T., Ooi E.H., Song C., "A Quadtree-Polygon-Based Scaled Boundary Finite Element Method for Crack Propagation Modeling in Functionally Graded Materials", Theor. Appl. Fract. Mech., Vol.94, 2018, pp.120–133.

[17] Chen, X., Chan, A.H., Modelling Impact Fracture and Fragmentation of Laminated Glass Using the Combined Finite-Discrete Element Method, Int. J. Impact Eng., Vol.112, 2018, pp.15–29.

[18] LI Jie , Zhang Xin, Huang Yuanjun, Sukang, Hu Bo, GuoJingbo," Numeral Analysis of Crack Initiation Life on Tunnel Boring Machine Cutter Seat", Jordan Journal of Mechanical and Industrial Engineering, Vol. 16, No. 5, 2022, pp. 653– 662.

[19] Zhipo Cao, Naixing Liang, Sheng Zeng , Xianshui Gang, "Dynamic Response Analysis of the Impact Force of Steel Wheel on the Elastic Half-Space", Jordan Journal of Mechanical and Industrial Engineering, Vol. 16, No.1, 2022, pp. 53 – 62.

[20] FadiAlfaqs, "Dynamic Behavior of Thin Graphite/Epoxy FRP Simply Supported Beam Under Thermal Load Using 3-D Finite Element Modeling", Jordan Journal of Mechanical and Industrial Engineering, Volume 15, Number 3, 2021, pp. 301 – 308.

[21] Jian-guang BAI , Hai-jun LI, "Numerical Simulation Study on Steel Pipe Row Pile Support of Temporary Road Slope", Jordan Journal of Mechanical and Industrial Engineering, Vol. 16, No. 5, 2022, pp.743– 752.

[22] G. Bolar, "3D Finite Element Method Simulations on the Influence of Tool Helix Angle in Thin-Wall Milling Process", Jordan Journal of Mechanical and Industrial Engineering, Vol. 16, No.2, 2022, pp. 283 – 289.

[23] Okodi A., Li Y., Cheng R., Kainat M., Yoosef-Ghodsi N., Adeeb S., "Crack Propagation and Burst Pressure of Pipeline with Restrained and Unrestrained Concentric Dent-Crack Defects Using Extended Finite Element Method", Appl. Sci. Vol.10, No.7554, 2020, pp.1-18.

[24] S. Wu, J. Qiao, J. Zou, "Effect of Microstructure and Stress Ratio on Fatigue Crack Propagation Behavior of A7N01 Aluminum Alloy Fiber Laser-VPTIG Hybrid Butt Welded", Opt. Laser Technol., Vol. 162, p. 109296, 2023, https://doi.org/10.1016/j.optlastec.2023.109296.

[25] X. Chen, A. Doitrand, N. Godin, and C. Fusco, "Crack Initiation in PMMA Plates With Circular Holes Considering Kinetic Energy and Nonlinear Elastic Material Behavior",Theor. Appl. Fract. Mech., Vol. 124, No.103783, 2023, pp.1-19.

[26] LI Jie, Zhang Xin, Huang Yuanjun, SU Kang, HU Bo, GuoJingbo, "Numeral Analysis of Crack Initiation Life on Tunnel Boring Machine Cutter Seat", Jordan Journal of Mechanical and Industrial Engineering, Vol.16, No. 5, 2022, pp.653– 662.

[27] LotfiChelbi, FatmaHentati, AmnaZnaidi, "Analysis of Fatigue Life and Crack Growth in Austenitic Stainless Steel AISI 304l", Jordan Journal of Mechanical and Industrial Engineering, Vol.17, No.4, 2023, pp. 501–508.

[28] Ehsan Rezaei, MehrdadPoursina , Mohsen Rezaei, AlirezaAriaei, "A New Analytical Approach for Crack Modeling in Spur Gears", Jordan Journal of Mechanical and Industrial Engineering, Vol. 13, No. 2, 2019, pp.69 – 74.

[29] Hadi Eskandari, "Three-Dimensional Investigations of Stress Intensity Factors in a Rotating Thick-Walled FGM Cylinder", Jordan Journal of Mechanical and Industrial Engineering, Vol. 10 No. 2, 2016, pp.105-113.

[30] NadhimM.Faleh,"The Effect of Tool Geometry for Resistance Spot Welds on Crack Growthin Specimens of Mild Steel", Eng. &Tech. Journal, Vol.31, Part (A), No.12, 2013, pp. 2242-2250.

[31] Dhafir S. Al-Fattal, Saif Khalid Mahmood, "Low Cycle Fatigue of Precipitation Hardened Aluminum Alloy", Eng. &Tech. Journal, Vol.33, Part (A), No.9, 2015, pp.2146-2158.

[32] Ziadoon M.R Al-hadrayi, Ahmed N. Al-Khazraji, Ahmed A. Shandookh, "Mathematical Model of Properties and Experimental Fatigue Investigation at Elevated Temperatures of Functionally Gradient Materials", Engineering and Technology Journal, Vol.41 , No.7, 2023, pp.940 -953.

[33] Shandong International Company Ltd., Shandong https://www.aluminumcoilsheet.com.

[34] R. Metz, "Impact and Drop Testing with ICP Force Sensors",Sound Vib., Vol. 41, No. 2, 2007,pp.18–20.

[35] Georgi P. Tolstov, Foureir Series, Dover publication Inc. New York: USA; 1962.

[36] T. K. Varadan, and K. Bhaskar. Analysis of Plates Theory and Problems, Department of Aerospace Engineering, India Institution of Technology. Madras: India; 1999.

[37] Stephen P. Timoshenko, and S. Woinowsky-Krieger. Theory of Plates and Shells. Second edition, New York, USA; 1986.

[38] MykhayloDelyavskyy, Krystian Rosinski. The New Approach to Analysis of Thin Isotropic Symmetrical Plates, Applied Sciences, Vol. 10, No. 5931, 2020, pp.1-36.